JOM, Vol. 66, No. 4, 2014
DOI: 10.1007/s11837-014-0940-0

Emissivity of Electronic Materials, Coatings, and Structures

SARANG V. MULEY[1] and NUGGEHALLI M. RAVINDRA[1,2]

1.—Interdisciplinary Program in Materials Science & Engineering, New Jersey Institute of Technology, Newark, NJ, USA. 2.—e-mail: nmravindra@gmail.com

This study presents an overview of commonly used electronic materials and nanocoatings, as well as the evolution and significance of emissivity of commonly used electronic materials and nanocoatings. In addition, some key issues are addressed, such as accurate temperature measurements during materials processing and control as well as thermal management in high-power electronic device applications. Case studies of the optical properties of bulk materials, multilayered structures, and electronic devices, mainly bolometers, are discussed and analyzed for optimization.

INTRODUCTION

In present-day manufacturing, industries that focus on materials processing have an acute requirement of temperature measurement encompassing a wide variety of applications. To address the needs of accurate process control in industry, various types of sensors and devices have been developed. The requirements of temperature monitoring can vary from as simple as the temperature of an engine or a device to as complex as knowing the temperature of a weld in laser welding applications. Some of the challenging applications that require temperature monitoring include the following: the measurement of temperature of steel in a blast furnace,[1] the exhaust of power generating stations, and emissions from rockets. Temperature measurement techniques can be classified as follows[2] and can be applied depending on the range and accuracy of measurement that is essential in a given process:

1. Thermometry
2. Probes
3. Noncontact probes

Thermometers are of two types based on the technique used: glass tube thermometers or bimetal thermometers. The accuracy of measurement depends, to a large extent, on the method of manufacturing as well as on the usage. Probes can be of various types. First, probes were resistance elements, which used the relationship between resistance and temperature for different elements, leading to the development of the thermistor.

Resistance temperature detectors (RTDs) were developed for higher accuracy; the device operates based on changing resistance in pure metals. Platinum RTD (PRTD) is the most accurate among these devices with a range of temperatures from −185°C to +480°C,[3] but its response is much slower and they have a higher cost. They are more suitable for low-temperature applications. Thermistors operate by changing electrical resistance with temperature; they are small and relatively low cost.

Thermocouples, which are formed by two dissimilar metals that are in physical contact with each other at one or more points, are another type of temperature sensors. They can be used to convert the temperature gradient into electricity based on the principle of the Seeback effect. The most important parameter in designing a measurement system is the dynamic response of its sensor. When a thermocouple is subject to rapid change in temperature, it will take some time to respond. If this response time is more than the rate of change of temperature, then the thermocouple used cannot be considered as ideal for representing the dynamic response to the fluctuations in temperature. The time constant characterizes the response of any function with respect to time. Each thermocouple has different time constants depending on the material and its size. Commonly used thermocouples are iron-constantan and copper-constantan; these thermocouples are relatively inexpensive.[4,5]

Noncontact temperature sensing is based on some form of radiative heat transfer measurement, i.e., detection of the heat radiated from a device. By measuring this heat, one can estimate its

(Published online March 28, 2014)

temperature from a distance of a millimeter to even millions of light years. These types of devices operate by permitting the radiation that is incident on an infrared sensitive element. Pyrometers are instruments used for in situ noncontact temperature measurements and can be used in applications such as processing silicon wafers or measuring the temperature of steel exiting a blast furnace. A schematic block diagram of operation of a typical radiation pyrometer is as shown in Fig. 1. Visible and infrared energy in the form of photons is emitted from the hot object. This energy is collected by an optical system that focuses it on to a detector, which converts the collected energy into an electrical signal to drive a temperature display or control unit. Two types of detectors generally used are thermal (thermopile) and photon (photomultiplier tubes) detectors, in which the latter are much faster than the former. Hence, to measure the temperature of small objects moving at fast speeds, one should use a photon-type detector.[6]

Challenging applications of noncontact temperature sensing techniques are pulsed laser ablation and rapid thermal processing (RTP). Pulsed laser deposition is a physical vapor deposition (PVD) technique using a high-power pulsed laser in high-vacuum conditions. In this technique, the material is vaporized from the target, wherein the incident laser pulse penetrates into the surface of the material. The depth of penetration is dependent on the laser wavelength and refractive index of the target material, with a value of about 10 nm for most materials. Pulsed laser irradiation is used widely in the rapid heating and cooling of surface layers, with a little increase of temperature in bulk materials. Temperature gradients, as a result of short pulse irradiation, yield a very high rate of surface cooling, which is usually studied in systems such as pulsed laser melting of silicon as well as during recrystallization of silicon on an insulator (in which heating is performed with electron beams of polycrystalline silicon to obtain single-crystal layers on insulator). Experimental data on temperature distribution due to the heating of silicon-on-insulator (SOI) materials are not easy to obtain because of the lack of suitable methods for temperature measurement with high spatial and temporal resolution. Conventional pyrometers and thermocouples are not capable of nanosecond-resolved temperature measurements over a large range of temperatures due to complex optical properties of the surface making emissivity unpredictable. Time-resolved reflectivity (TRR) is a method used to study such temperature distributions across the SOI films and can overcome the limitations by aiding in characterization of scanned beam heating of the substrates.[7]

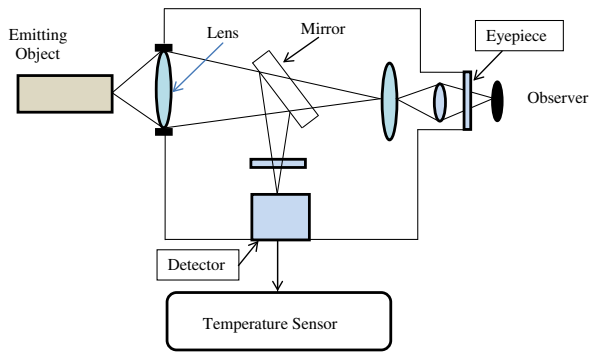

Fig. 1. Block diagram of a radiation pyrometer.

RTP is a widely used technique for the manufacture of silicon devices, wherein short process times, high-temperature ramp rates, and very high temperatures are essential.[8] During this process, temperature uniformity across the surface of the wafer, process repeatability, reproducibility, and accuracy are keys to its successful operation. Temperature uniformity across the wafer is affected by design parameters such as wafer patterning, temperature accuracy, and uniformity of irradiation. Temperature accuracy depends on the technique used for the measurement. The use of thermocouples in temperature measurement is highly intrusive; the delicate thermocouple wires make handling of wafers especially difficult and pose problems in sealing vacuum chambers.[9]

In this regard, pyrometers are the most suitable choice of temperature-measurement techniques.[10] Pyrometers can be used to measure the amount of radiation emitted within a narrow window of wavelength. However, to obtain an accurate measurement of temperatures using these devices, one should have knowledge of some key optical properties of the material that is being analyzed. Spectral emissivity is defined as the ratio of the radiation emitted by a given substrate to that of a blackbody under the same conditions of temperature, wavelength, angle of incidence, and direction of polarization. It is a number between 0 and 1. It takes into consideration the wavelength, transmittance, absorptivity, absorption coefficient, reflectivity, and so on.[11] Ratio pyrometry is a technique of radiometric method that is used to eliminate like terms from ratios of measured signals. Multiwavelength imaging pyrometers (MWIPs) are designed to obtain temperature profiles, remotely, of targets of unknown wavelength-dependent emissivity. MWIPs are based on the measurement of the temperature and the emissivity, simultaneously, from the least-squares fit of the signal taken from the radiometric model of an infrared (IR) camera. The accuracy of the least-squares-based MWIP technique of measurement is dependent on the emissivity model selected.[12,13]

The radiative properties of materials are of significant interest in applications such as materials process monitoring and control, noncontact temperature sensors, pyrometry, infrared detectors including bolometers, night vision, and so on.[11] These properties are not easily available in the literature, and the results presented in this study can

be helpful in various applications including thermal management of high-power electronic devices. The need for having apt thermal management in electronics has led to the development of alternative materials, techniques of manufacturing, and designs to have a higher lifecycle of the electronic devices; the cost is also a serious consideration.

THERMAL MANAGEMENT IN ELECTRONICS

The electronic revolution in the twentieth century started with silicon as a first generation semiconductor, followed by application of second-generation III-V group semiconductors, mainly GaAs and InP, during the wireless revolution. At the start of the twenty-first century, GaN and SiC, which are wide-bandgap semiconductors, are being used in opto-electronics applications in making blue light-emitting diodes (LEDs). There are several advantages of using SiC devices. The developed device fabrication technology uses Diamond, which is another wide-bandgap semiconductor (5.5 eV). It is the topic of research in recent times, which is driven by the need for light emitters. It can be used in high-temperature and high-power device applications in aircraft and space systems, deep well drilling, energy production centers, electronics in automotives, and so on.[14]

Approaches to thermal management, being used currently, introduce additional overhead because the performance-enhancing electronics, which are used to monitor the crucial hot components, must be present in cooler areas. Therefore, these parts require longer connecting wires and plumbing for the cooling systems, resulting in increased complexity. Some of the critical problems in using the present-day Si power devices for temperatures greater than 200°C are the self-heating on account of flow of high current at high power levels (causing leakage) and very high junction temperatures internally in the devices.[15]

Electromigration is the gradual movement of ions in a conductor due to the transfer of momentum between electrons and diffusing metal atoms. This effect is of high significance in microelectronics and related structures in which high current densities are used in relatively small areas due to the miniaturization of the circuits. It decreases the reliability of integrated circuits (ICs) and can cause eventual failure of circuits. The most common conducting material used in silicon ICs is aluminum because of its physical and chemical properties such as good conductivity, the ability to adhere to the substrate, and the ability to form Ohmic contacts with silicon; however, it is highly susceptible to electromigration. The reliability of circuits can be improved by either doping aluminum with about 2–4% copper or replacing it entirely with copper; the latter can withstand higher current density than aluminum.[16,17]

The following examples will be discussed in this study: silicon on insulator, silicon on diamond (SOD), silicon on sapphire (SOS), silicon on calcium fluoride, and carbon-like materials.

Silicon on Insulator

Silicon on insulator (SOI) is a substrate-engineered concept and was proposed around 1980 for improving the performance of metal-oxide semiconductor (MOS) devices leading, in particular, to thermal management and confinement of charge[15] mainly in niche areas such as high-temperature electronics, aerospace, and military applications.[18] In SOI, a thin film of single-crystal silicon is formed on top of electrically insulating silica, which in turn is present on top of a thick silicon handling wafer. "Latch up" is a type of short circuit occurring in improperly designed ICs, specifically leading to the creation of low impedance path between power supply rails of metal oxide semiconductor field-effect transistor (MOSFET) circuits, triggering a parasitic structure disrupting proper functioning of the part on account of overcurrent. In complementary metal-oxide semiconductor (CMOS) technology, there are a large number of intrinsic bipolar junction transistors, which can create problems when *n*- and *p*-wells, combined with the substrate, lead to formation of *n-p-n-p* type of parasitic structures. The possible way to prevent this is to design chips in which a layer of insulating oxides surrounds the transistors. Most of the SOI devices are inherently latchup resistant.[19]

Some of the techniques to develop SOI are based on epitaxial growth and are termed as homoepitaxial techniques in which an epitaxial layer of silicon is grown on a silicon wafer covered with an insulator or heteroepitaxial technique if it is grown on a crystalline insulator. Many techniques have been developed for producing single-crystal silicon on insulator. SOI can be produced from wafer of bulk silicon by isolating a layer of thin silicon from the substrate by the formation or oxidation of porous silicon (FIPOS) or through ion beam implantation of oxygen into silicon (SIMOX).[18]

The SOI material can also be obtained by performing a thinning operation of a silicon wafer bonded to an insulator and a mechanical substrate (BESOI). Thin-film SOI (TFSOI) devices have been adopted by major chip manufacturers as they can potentially overcome some of the key issues in silicon CMOS ICs, such as reduced junction areas, simplified isolation, and steep slopes of subthreshold regimes. They enhance low-voltage operation and simplify fabrication of circuit.[15]

However, optical characterization of SIMOX has been a challenge because of the complexity of built-in multilayers. Significant efforts have been made in the literature to investigate the optical properties of SIMOX. Also, the electrical characteristics of SIMOX buried oxide are inferior to that of thermally grown silica. The most important distinction between SIMOX buried oxide and thermally grown oxide is the presence of excess silicon in the former case.[18]

High-temperature electronics require high temperature stability, high breakdown field, high thermal conductivity, and high chemical stability so as to decrease power losses, volume, and weight of the system along with its associated cost. These unique properties for high-temperature and high-power applications can be achieved by using wide-bandgap semiconductors that have better physical and chemical characteristics than devices fabricated from silicon. Diamonds have better properties in this regard than most other materials proposed for power electronics at high frequencies and high temperatures. However, the challenging area is the method of production of thin films of diamond over a large area at low cost and single-crystal film with low defect density.[14]

Silicon on Diamond

SOD is a candidate for the next generation of SOI materials, which is an alternative SOI concept in which thermally insulating silica has been replaced by high thermal conductive diamond.[20] Silicon on diamond (SOD) is achieved by joining thin single-crystal Si device layer to a highly oriented diamond (HOD) serving as an electrical insulator, heat-dissipating layer, and supporting substrate. Below 600 K, undoped diamond is a highly insulating material. Diamond has conductivity about 10 times that of silicon and about 1,000 times that of silicon dioxide. The SOD approach has been shown by Soderbarg et al.[21,22] to be compatible with the present-day silicon device fabrication technologies and has demonstrated the fabrication of ICs without degradation and cross contamination. Gu et al.[23] have transferred the concept of SOD to 4-in. wafers, aiming to improve radiation hardness of SOD with respect to silicon.

Silicon on Sapphire

Silicon on Sapphire (SOS) has been used since the 1960s for applications such as rad-hard electronics because of the full dielectric nature of the substrate.[24] They are produced by epitaxial growth of silicon on (1 1-1 2)-oriented crystalline alumina (sapphire) wafer. Because of the lattice mismatch between silicon and sapphire, the density of defects in the as-grown silicon film is high and is usually in the form of stacking faults and (micro) twins, which ultimately result in low values of resistivity, mobility, and lifetime near the interface. The low electron mobility at the Si-sapphire interface results in reduction of back-channel leakage current in *n*-channel devices.[18] Three-dimensional circuits have been studied and successfully fabricated for applications such as a moving object detector, a character recognition system using laser, or an e-beam recrystallization leading to the formation of SOI devices on top of processed devices via heteroepitaxial growth of silicon. Solid-phase epitaxy and regrowth (SPEAR) and the double solid-phase epitaxy (DSPE) techniques are some of the important methods for improving the crystalline quality of SOS films.[24]

Silicon on Calcium Fluoride

Silicon on calcium fluoride is another SOI structure, which is produced by epitaxial growth of CaF_2 on silicon. However, because of the difference in thermal expansion coefficients and lattice mismatch of silicon and CaF_2 over an appreciable temperature range, it is common to grow essentially stress-free silicon on top of calcium fluoride with a bottom support of silicon wafer using molecular beam epitaxy or e-beam evaporation at about 800°C.[18]

Carbon-Like Materials

Because of the continued trend in miniaturization of electronic devices, densified heat that is generated from parts of the device is likely to increase in the future. The heat generated by these components is not effectively dissipated to the surroundings, leading to overheating of electronic components, and ultimately, it begins to malfunction. Some of the available approaches for thermal management of devices are using in heat sink and fan arrangements. A recent approach for heat transfer based on radiative cooling has led to the development of molecular fan (MF) coating with high surface emissivity (emissivity value of about 0.98 with respect to emissivity = 1 for a blackbody) for effective heat dissipation in electronic devices.[25] For high-power and high-brightness LEDs, an inefficient heat-dissipation device can cause heating problems leading to lower light efficiency and lesser lifetime of the device. Carbon-based materials such as diamond and in-plane graphite have been known to have high thermal conductivity values with thermal transport being dominated by phonons. Graphene (a single layer of carbon atoms of graphite in honeycomb lattice) is known to have extremely high thermal conductivity (as high as 10000 W/mK predicted by molecular dynamics simulations and about 5000 W/mK measured experimentally), which is caused by a large mean free path of phonons in graphene. The high values of thermal conductivity have been the driving force for use of carbon based materials for thermal management applications.[25]

Graphene has been found to exhibit unique electronic properties.[26] An ultrathin two-dimensional layer of graphene permits ideal electrostatics for an ultimately scaled down device.[27] Graphene has extremely high quantum efficiency for interactions of light matter and is strongly optically nonlinear.[28] Along with excellent thermal and electronic characteristics, graphene is found to have unique mechanical properties and is about 300 times stronger than steel. Graphene is found to have a very high transmittance (about 85–90%) along with a very low value of emissivity (about 2.3%) in the visible to near-IR region of the optical spectrum. These novel properties of graphene make it suitable

Table I. Thermal conductivities of various materials used in electronics[14,30–32]

Material	Thermal conductivity (W/mK)
Diamond	1000–2000
Graphite	25–470
Graphene	5000–1000
Silicon	150
SiC	490 @ 295 K
GaAs	80
GaN	140
CaF_2	6.9
Sapphire (Al_2O_3)	27.21 @ 300 K

as one of the thin-film layers in optoelectronic devices.[29] Table I shows the thermal conductivity values for various materials of importance in electronics.

IMPORTANCE OF COATINGS AND MULTI-LAYERED STRUCTURES IN ELECTRONICS

In an industrial environment, there is a growing need to control or reduce friction and wear, as well as the corrosion of its components, to extend the life of the device, conserve scarce material resources, save energy, and improvise safety in engineering applications. Nanocoatings such as thin films and engineered surfaces have been developed and applied in industry for decades. Highly improvised surface-related characteristics such as optical, magnetic, electronic, and catalytic properties can be obtained via nanocoatings. There are two types of coatings based on the severity of applications: active coatings, which are electrochromic, thermochromic, photochromic, or magnetochromic, and passive coatings, which are used mainly to address the issue of corrosion as well as hydrophilicity of materials in working environment. Electrochromic coatings, i.e., thin films that change their optical absorptance or reflectance as a function of injected ions (H^+ or Li^+ ions), can be applied for products such as smart windows, switchable motorcycle helmets, nonemissive large area color displays for advertisements, and antidazzling rear view mirrors.[33] They are applied in ophthalmics, architectural glazing, instrumentation devices, and displays.[34] Thermochromic material coatings are applied to avoid overheating in applications such as solar thermal collectors that are used as renewable energy sources for domestic hot water production and space heating. Photochromic coatings change their color reversibly by action of light and can be applied in light sensors in optical devices and decoration of windows. Hybrid coatings can have appropriate porosity and surface activity that is essential to obtain both photochromic as well as thermochromic effects.[35]

The presence of thin films on a substrate causes a large fluctuation in the spectral reflectivity. A typical example is the presence of an oxide layer on top of silicon wafer surface that causes lower reflectivity due to thin-film interference and, consequently, an increase in total absorptivity as well as emissivity. For very thin films, the optical properties approach that of the substrate. However, multilayered films on wafers produce a dramatic change in spectral reflectivity of the wafer. In this case, the net effect on properties is less predictable and one could even observe a reduction in emissivity with respect to the bare substrate. At high temperatures, for thin-film structure, the change in spectral reflectivity follows changes in the surface conditions of the silicon substrate along with a shift in the bandgap absorption edge. The deviation in properties depends on the layer thickness of the films, surface roughness or incident range of wavelengths. Various software programs such as Multi-Rad[36–39] and Scout[40] have been developed to simulate the wavelength dependence of emissivity, transmittance and reflectance as a function of thickness of various layers in the structure. In this work, the simulation of the radiative properties of materials is based on Multi-Rad.

THIN FILMS AND OPTICS

When light is reflected in a thin film, both the boundaries, one of top surface and the other of the interface, have to be taken into account. In a thin layer, light will be reflected back at the secondary boundary, followed by transmission through the first boundary. Hence, there will be a path difference between the two waves (one traveling inside and one reflected from the surface), and thus phase difference is observed, resulting in interference of the waves. Hence, the reflectance is highly dependent on the thickness of the films and the wavelength of light. In Scout software, Fresnel's equations are used for studying the reflection and transmission of electromagnetic waves at the boundary.[40]

Multi-Rad software was originally developed at Massachusetts Institute of Technology (MIT) for performing the calculations of the radiative properties of silicon related materials and structures. In the present study, it has been used for calculating the radiative properties of thin-film stacks. In Multi-Rad, the thin film optics has been implemented in the form of matrix method of multilayers. The model assumes the following: (I) the layers are optically smooth and parallel, and materials are isotropic; and (II) constancy of the properties in azimuthal direction. For a given multilayer stack, one can calculate the radiative properties as a function of wavelength and angle of incidence, at a specific temperature.[38] A material is defined using its refractive indices n and extinction coefficients k. Most of these fundamental optical parameters in our studies have been based on Refs. 41–43.

The matrix method of multilayers is useful in predicting the reflectance and transmittance of a

multilayer stack for a specific wavelength and angle of incidence. For a specific wavelength, the radiation is treated as coherent so as to take interference effects into consideration. One important assumption of this theory is that the area of the surface on which the radiation is incident is much larger than the wavelength of the incident radiation (i.e., no edge effects).[39]

A schematic of the layered structure is shown in Fig. 2. N layer interfaces (circled) and $N + 1$ "layers" (squared) are shown, including the unbounded transparent media on each side of the actual stack. A_i and B_i are the respective amplitudes during the forward and backward propagation of electric field vectors on the left side of the interface i. The prime notation on A'_{N+1} and B'_{N+1} indicates that these are the amplitudes on the right side of the interface N. Incident radiation on interface 1 is at an angle of incidence $\theta 1$ to the normal.

The equation, based on multilayer theory, which relates the amplitudes on the left side of interface 1 with the amplitudes on the right side of interface N, is:

$$\begin{pmatrix} A_1 \\ B_1 \end{pmatrix} = \left[\prod_{i=1}^{N} P_i D_i^{-1} D_{i+1} \right] \begin{bmatrix} A'_{N+1} \\ B'_{N+1} \end{bmatrix} = \begin{bmatrix} m_{11} & m_{12} \\ m_{21} & m_{22} \end{bmatrix} \begin{bmatrix} A'_{N+1} \\ B'_{N+1} \end{bmatrix}, \tag{1}$$

where P_i is the propagation matrix, D_i is the dynamical matrix, and m_{ij} is an element of the transfer function matrix. Detailed derivation of reflectance and transmittance using this theory has been described in the literature.[39]

The spectral directional absorptance is calculated by subtracting the reflectance and transmittance from unity, and the spectral directional emittance is calculated by assuming Kirchhoff's law on a spectral basis:

$$\alpha_{\lambda,\theta} = \varepsilon_{\lambda,\theta} = 1 - R_{\lambda,\theta} - T_{\lambda,\theta}, \tag{2}$$

where the subscripts λ and θ have been introduced to indicate spectral and directional properties, respectively. Spectral directional reflectance and transmittance are denoted, respectively, as $R_{\lambda,\theta}$ and $T_{\lambda,\theta}$ and can be calculated from the average of s and p wave properties. If it is assumed that a given emitter is in local thermodynamic equilibrium, then Kirchhoff's law is valid on a spectral basis, which is characterized by a single temperature. In case of high gradients of temperature across the emitting wafer, or if the electrons and phonons are not in local thermal equilibrium, then Kirchhoff's law is not valid.

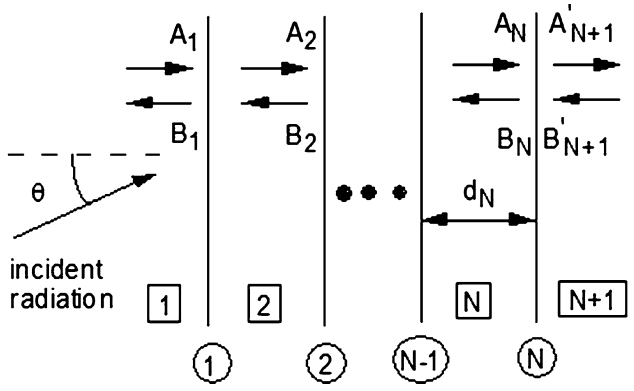

Fig. 2. Schematic for matrix method of multilayers.[38]

CASE STUDIES

Three case studies have been presented in this work, as follows:

1. Bulk materials analysis
2. Multilayered structures
3. Device applications

Case 1: Bulk Materials Analysis

In this case, we compared the optical properties of emissivity, transmittance, and reflectance spectra of materials that are of significant importance in electronics.

Bulk Silicon and Aluminum

The most commonly used materials in electronics industries are silicon and aluminum. Figure 3 shows a plot of emissivities for commonly used thicknesses of bulk Al and Si in the wavelength range of 1–20 μm. It is observed that in the case of aluminum, the emissivity is almost constant at about 0.01 for all the thicknesses considered, 0.1–5000 μm. This is a typical metallic absorption spectra in the IR, as three electrons per atom contribute to the conduction band from the valence band levels $3s^2 3p$ in the energy range of 0–15 eV. The portion of spectrum of Al in the far infrared, i.e., beyond 2.5 μm, is dominated by intraband absorption, with two strong absorption bands at about 2.5 μm and 0.8 μm.[41] This feature is shown in Fig. 3a at 2.5 μm. Wiedemann–Franz law can be applied for calculating the thermal conductivity of pure aluminum, relating it with the electrical conductivity. In the case of silicon, as shown in Fig. 3b, it is found that the emissivity increases from a negligibly small value to about 0.7 with increase in thickness of bulk silicon from 0.1 μm to 5000 μm. The plot of emissivity versus wavelength for silicon shows a significant peak at about 16.5 μm, which increases with increasing thickness of silicon.

Carbon-Like Materials: Diamond, Graphite, and Graphene

Carbon allotropes are finding significant applications in electronics because of their excellent physical, mechanical, electronic, and electrical properties. As can be seen in Fig. 4a, emissivities of bare substrates of carbon allotropes, natural diamond, and graphite for different thicknesses, in the

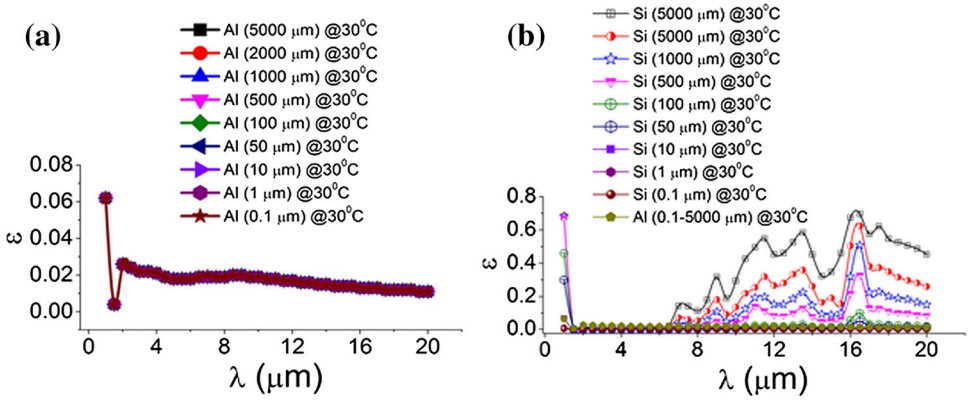

Fig. 3. Emissivity versus wavelength (1–20 μm) for (a) bulk aluminum for thickness from 0.1 μm to 5000 μm, (b) various thicknesses of silicon (0.1–5000 μm) and of aluminum (0.1–5000 μm) (temperature in °C).

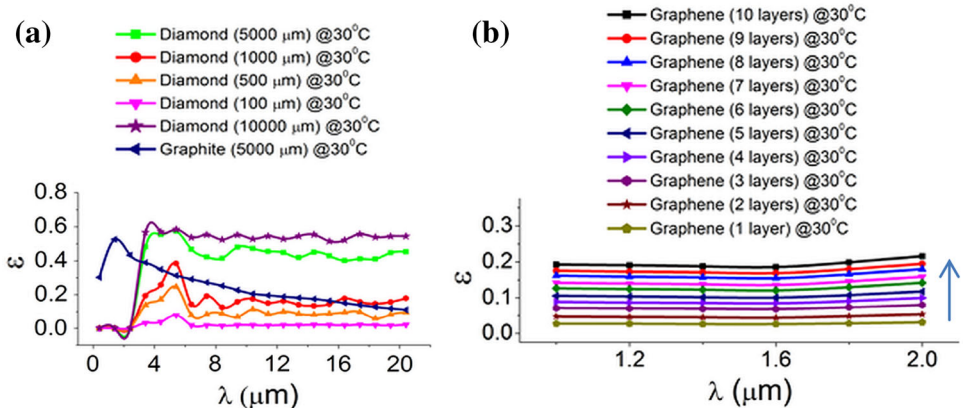

Fig. 4. (a) Emissivity versus wavelength for diamond and graphite, and (b) emissivity versus wavelength for graphene up to 10 layers (temperature in °C).

wavelength range of 0.4–20 μm, have been compared. It is noticed that the emissivity increases with an increasing thickness of the diamond in the range of 500–5000 μm from 0 to ~0.6. For the same range of thickness, i.e., 500–5000 μm, absorption in graphite is found to follow a single trend rising from 0.3 μm at 0.43 μm to 0.48 at 1.7 μm, and then the emissivity values decrease linearly to ~0.11 at 20 μm. Among the thicknesses considered, the emissivity of diamond is found to be the highest for a thickness of 5000 μm, showing the trend of increasing linearly with wavelength from about 0 at 0.4 μm to 0.57 at 4 μm wavelength.

Figure 4b shows emissivity versus wavelength for graphene as well as few layers of graphene (FLG) at room temperature, which is found to be almost constant with respect to wavelength in the range of 1–2 μm (temperature in °C).

Single-layer graphene is found to absorb ~2.3% of the incoming IR radiation, theoretically as well as experimentally, which is attributed to the interband absorption in a wide range of wavelengths spanning from the visible to infrared.[44] The values obtained from our calculations are found to be ~2.5% (as can be seen in the emissivity plot in Fig. 4b) for single-layer graphene, which is found to increase to ~20% with increasing number of layers to 10. Graphene has a very low reflectivity, and most of the incident electromagnetic waves are found to be transmitted (about 97%).

Materials for Optical Windows: Calcium Fluoride (CaF_2) and Sapphire (Al_2O_3)

Because of the high average transmission and lower chromatic aberration with respect to other IR materials, calcium fluoride is an excellent option for optical windows and lenses for applications in spectroscopy. In Fig. 5, a comparison of the emissivity, transmittance, and reflectance for thicknesses (ranging from 1 μm to 2000 μm) of calcium fluoride and sapphire, at room temperature, is presented for the wavelength range of 1–20 μm.

It can be noted that in case of CaF_2, the transmittance is ~1.0 up to a wavelength of ~6.5 μm, whereas it decreases to a negligible value in the range of 10–20 μm. It shows a trend of decreasing transmittance with increasing thickness of CaF_2 as shown in Fig. 5a. The emissivity of CaF_2 is found to

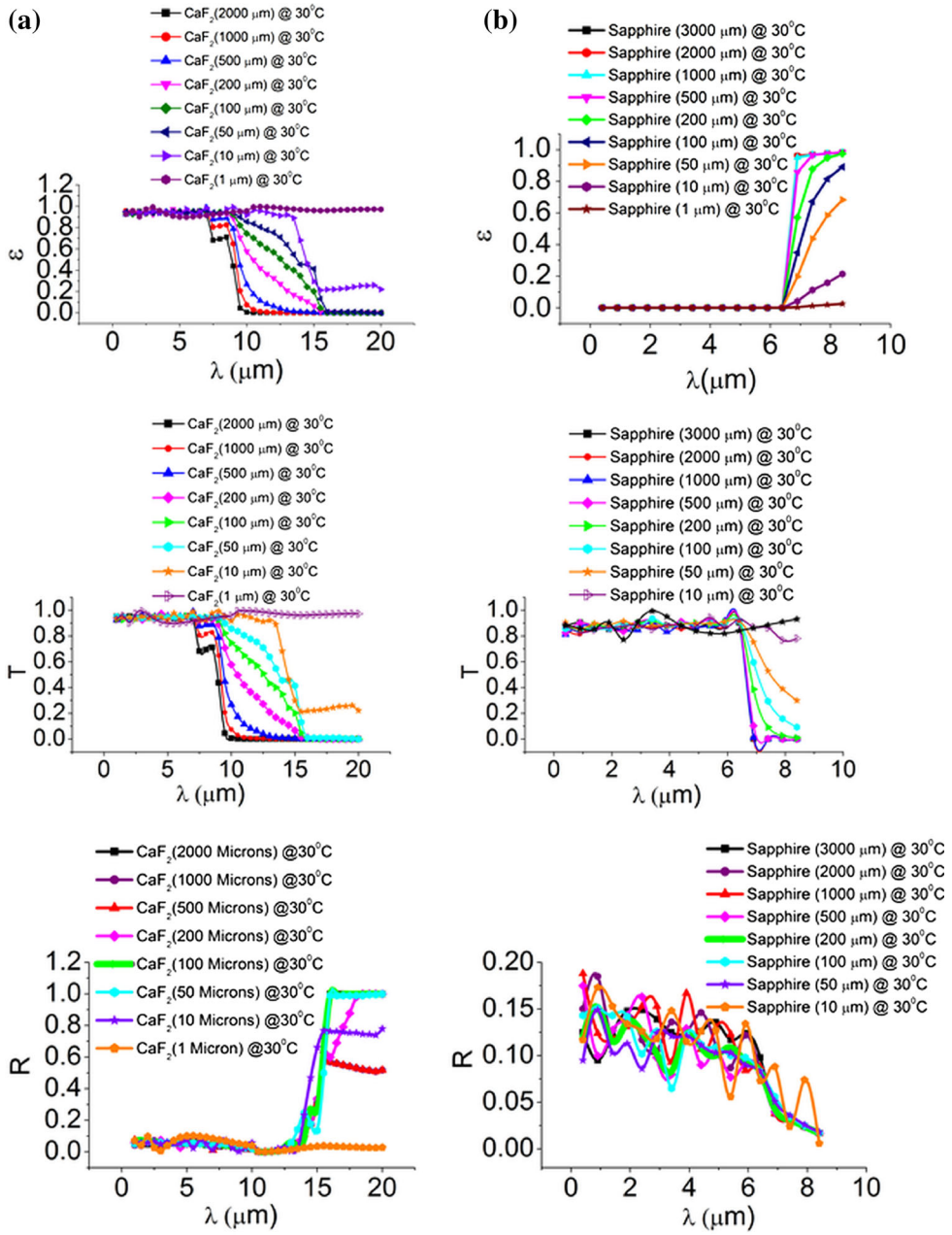

Fig. 5. Emissivity, transmittance, and reflectance-versus-wavelength plots for calcium fluoride and sapphire for varying thicknesses at room temperature (in °C).

increase with thickness and reaches a peak value in the wavelength range of 8.5–15 μm.

In the case of sapphire, it is found that the emissivity curves follow a trend such that all the thicknesses of sapphire exhibit negligible and constant emissivity in the wavelength range of 1–6 μm as shown in Fig. 5b. Emissivity reaches its peak value of 1.0 at a wavelength of $\sim$7 μm and exhibits constancy up to 8.5 μm. The corresponding transmittance for sapphire is found to have constant values of 0.98 up to wavelength of $\sim$6 μm, independent of thickness, and it is found to decrease at a wavelength of 7.5 μm.

Thus, as expected, it is seen that both sapphire and CaF_2 are ideal infrared windows in the wavelength range of 1–7.5 μm.

Materials Used for Manufacture of Blue LEDs (SiC and GaN)

As noted, silicon carbide and gallium nitride are the materials that are used widely for the manufacture of blue LEDs. In Fig. 6a, we have presented a study of the comparison of emissivity, transmittance, and reflectance spectra for silicon carbide and gallium nitride for varying thicknesses. It is clear

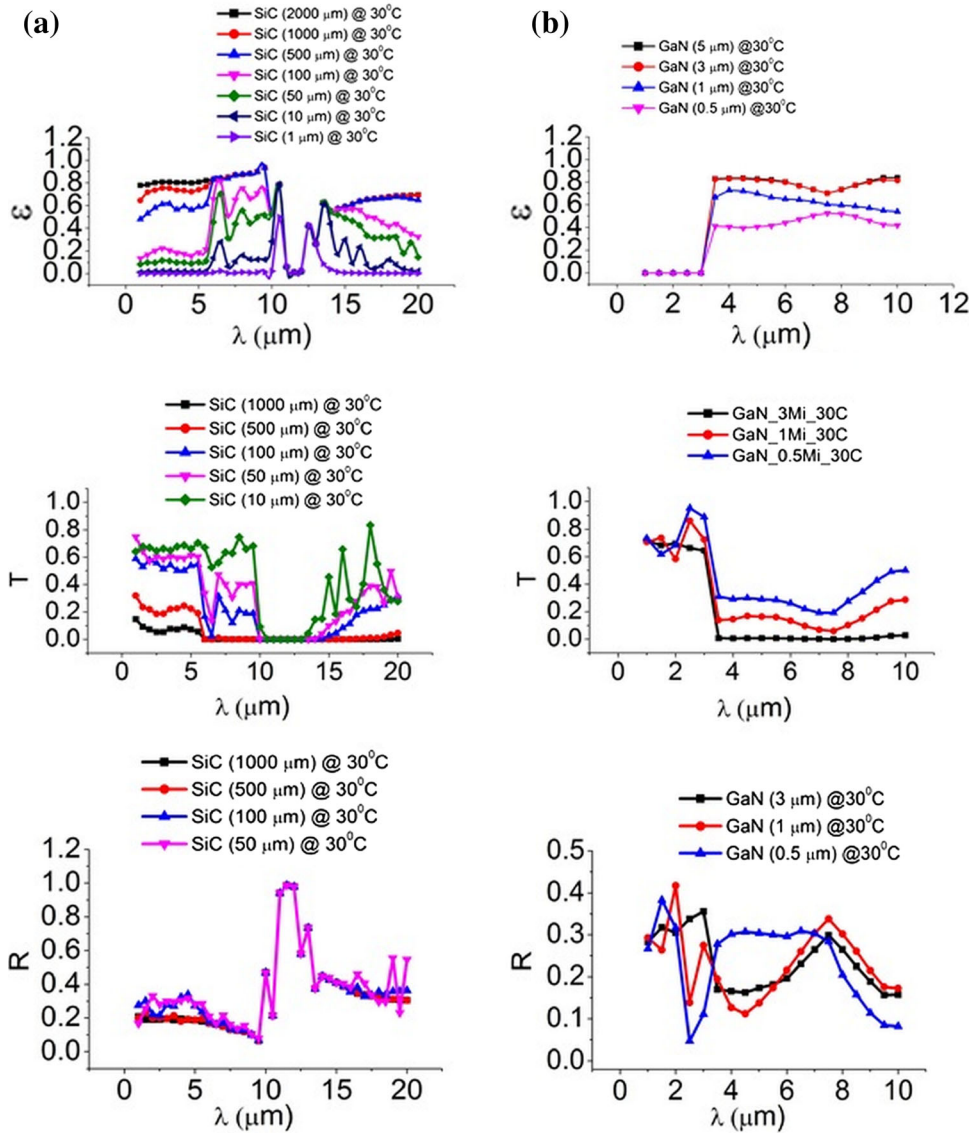

Fig. 6. Emissivity, reflectance, and transmittance as a function of wavelength for (a) SiC and (b) GaN.

that emissivity increases with increasing thickness of silicon carbide, and it is found to follow the same trend for thicknesses higher than 500 μm, with certain deviations in wavelengths below 5 μm and beyond 15 μm. It is noted that for silicon carbide, emissivity reaches ~0.8–0.98 in the wavelength range of 1–9.3 μm for thicknesses higher than 500 μm, whereas it is found to have a negligible value (~0.024) at 11.6 μm. Corresponding transmittance shows a negligible value from ~10.5 μm to 13 μm, and a reflectance plot shows a peak at ~11.6 μm with values lower on either side of the peak. Reflectance is found to follow the same trend for all the thicknesses from 50 μm to 1000 μm, with certain deviations below ~9.6 μm and above 13.7 μm wavelengths. The reflectance spectra of SiC is found to exhibit a peak in the wavelength range of ~10.5–13 μm with a value of ~0.9–1.0, whereas it decreases to ~0.1–0.5 in the rest of the wavelength range. This is found to be in accord with the experimentally determined reflectance in the literature.[45]

Similarly, as seen in Fig. 6b for gallium nitride, emissivity increases with an increase in thickness from 0.5 μm to 5 μm in the wavelength range of 3–10 μm. It is observed that there is no change in emissivity for thicknesses beyond 5 μm for GaN, and it saturates to an emissivity value of about 0.89. Also, a constant increase in emissivity is to be noted beyond 3-μm wavelength in all the cases. As seen in the transmittance plots, an increase in thickness beyond 3 μm leads to constant and low transmittance at wavelengths in the range of 4–10 μm.

Case 2: Multilayered Structures

As discussed in the section pertaining to thermal management of high-power electronic devices, it is essential to obtain accurate values of their

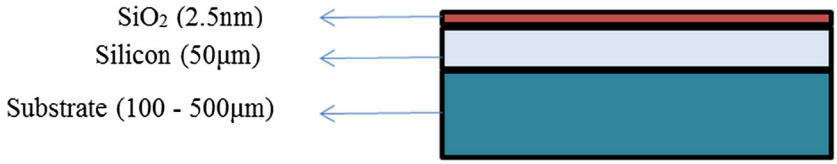

Fig. 7. Multilayered structure simulated for SOD, SOI, SOS, silicon on graphite, and silicon on graphene.

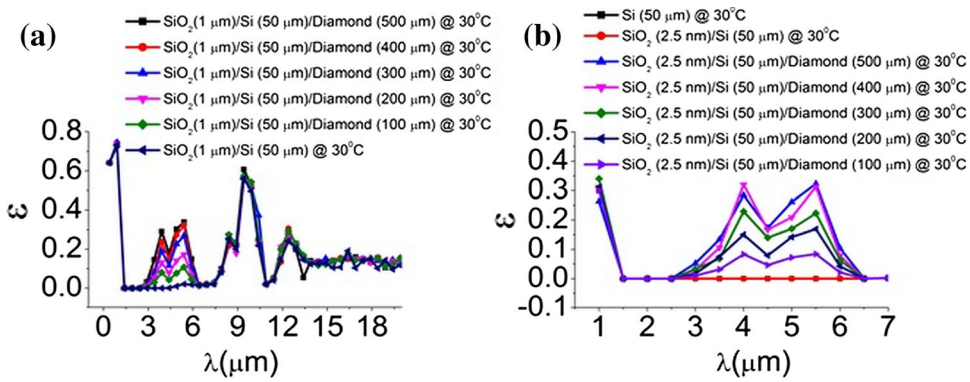

Fig. 8. Effect of variation of thickness of SiO_2 on emissivity versus wavelength for (a) SiO_2(2.5 nm)/Si(50 μm)/diamond (100–500 μm) and (b) SiO_2(1 μm)/Si(50 μm)/diamond (100–500 μm) (temperature in °C).

temperature in specific spectral range. This leads to the application of noncontact temperature-sensing devices such as pyrometers. Accurate values of wavelength and temperature-dependent emissivity of a given material or structure are essential to obtain temperatures using pyrometers. Here, we present the trends in optical properties in the IR wavelength range in case of SOD, SIMOX, SOI (Si on CaF_2), SOS, silicon on graphene, silicon on graphite, and graphene on silicon. We have considered a multilayered structure as shown in Fig. 7, in simulations of the optical properties of SOD, SOI, SOS, silicon on graphene, and silicon on graphite. The variation in optical properties with changing substrate thickness from 100 μm to 500 μm has been shown.

Silicon on Diamond

We have simulated the structure as shown in Fig. 7 using diamond as the substrate at room temperature, and the corresponding plots are shown in Fig. 8a. To study the effect of the variation of thickness of silica on emissivity, we have used a silica layer thickness of 1 μm instead of 2.5 nm, and the corresponding results are shown in Fig. 8b. The plots for SOD structure are compared with bare silicon (50 μm) and SiO_2/Si for understanding the variations in emissivity with the addition of the diamond layer as a substrate. It is clear from the plots that at room temperature, the emissivity increases with an increase in thickness of diamond, with all other parameters kept constant. Also, it follows a trend showing a decrease in emissivity for wavelengths greater than 7.5 μm. A comparison of Fig. 8a and b clearly indicates that an increase in the silica layer thickness leads to enhanced emissivity to 0.6 at 9.5 μm, which can be considered as a signature peak of silica. Also, the emissivity increases in longer wavelengths due to the presence of the silica layer of 1 μm thickness.

To study the effects of minor variations of silica layer thickness at higher processing temperatures (about 200°C), keeping the same substrate (i.e., diamond) thickness of 200 μm for all cases shows that there is no change in the emissivity of SOD structure in the wavelength range of 1–20 μm as shown in Fig. 9.

It is observed in Fig. 10 that the emissivity saturates at about 0.7, which is the same as that for pristine silicon at 800°C. To study the effect of the absence of silica layer on the top, we simulated the structure as in Fig. 7, using diamond as the substrate with thicknesses varying from 50 μm to 100 μm and silicon layer thickness is taken as 1 μm (to consider the effect of thin film of SOD). The corresponding results of emissivity versus wavelength (1–20 μm) are shown in Fig. 11.

It is found that the emissivity increases with thickness of diamond from 50 μm to 100 μm, keeping the silicon layer thickness constant. Also, there is no peak in longer wavelength regions because of the absence of silica.

SIMOX

We have simulated the optical properties of the SIMOX (Si/SiO_2/Si) structure as shown in Fig. 12.

The substrate thickness has been varied from 100 μm to 500 μm.

Trends in the variation of optical properties have been observed for the SIMOX structure as a function of temperature at 30°C, 200°C, 400°C, 600°C, and 800°C as shown in Fig. 13.

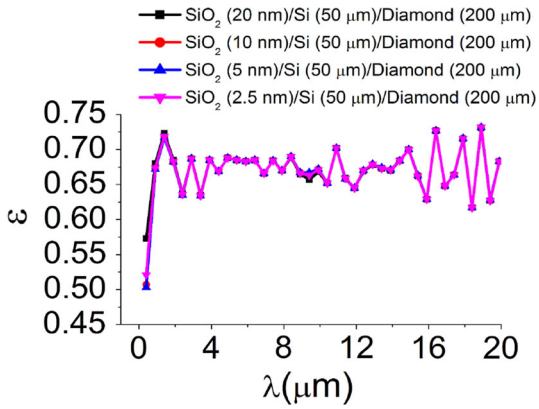

Fig. 9. Effect of variation of silica thickness (2.5 nm, 5 nm, 10 nm, and 20 nm) on silicon (50 μm)/diamond (200 μm) at 200°C.

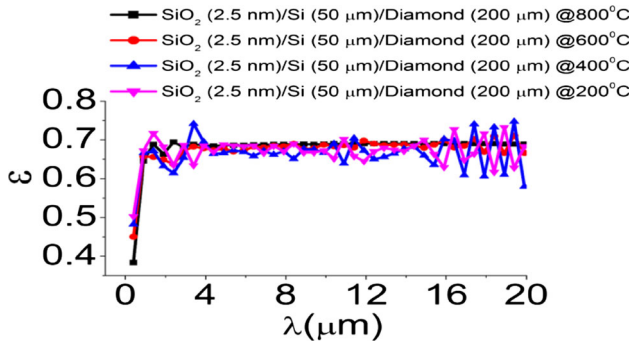

Fig. 10. Emissivity-versus-wavelength plot of SiO_2 (2.5 nm)/Si (50 μm)/diamond (100–500 μm) (temperature in °C).

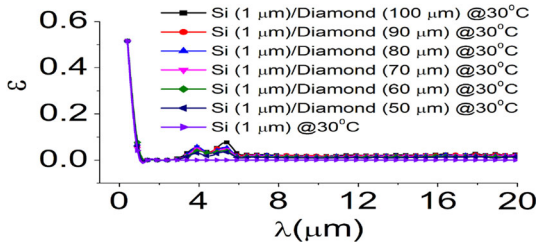

Fig. 11. Emissivity-versus-wavelength plot of Si (1 μm)/diamond (50–100 μm) (temperature in °C).

It is observed in Fig. 13 that by increasing the thickness of the silicon substrate, at room temperature, the peak emissivity of about 0.4 is noted at ~9.5 μm wavelength and another small peak at ~12.5 μm with emissivity of 0.25, followed by a major peak at a wavelength of ~16.4 μm with emissivity of 0.4 for a silicon wafer thickness of 500 μm. It is also evident from the corresponding plot of transmittance as a function of the wavelength. With an increase in temperature, it is seen that the peak emissivity at 16.4 μm is reduced to ~0.35, with no other major changes in its behavior at room temperature. At 400°C, the peak emissivity increases by ~0.2 over the original values at wavelengths of 9.5 μm and 16.4 μm, whereas transmittance is found to decrease by almost an equivalent factor for the respective wavelengths. At 600°C, peak transmittance is observed at a wavelength of 1.55 μm with a value of 0.37, whereas the emissivity exhibits a steep slope at ~2.5 μm, and the emissivity peak is observed at 7.89 μm with a value of 0.97. With an increase in temperature, one can observe a trend in emissivity versus wavelength. The emissivity values are independent of thickness of silicon substrate for higher temperatures, whereas transmittance continues to decrease with increasing thickness of substrate at the same temperatures. Our simulated results of emissivity are found to be in good agreement with the experiments.[15]

Silicon on Insulator ($SiO_2/Si/CaF_2$)

We have simulated a multilayered structure as in Fig. 7 with calcium fluoride (100–500 μm) as the substrate, and the corresponding results of emissivity and transmittance are plotted and shown in Fig. 14 in the wavelength range of 1–15 μm.

It can be noted from Fig. 14 that the emissivity values of silicon on insulator (calcium fluoride) are negligible in the wavelength range of 1–8.5 μm, while it increases with increase in wavelength in the range of ~8.5–15 μm with peak emissivity varying from 0.3 to 0.6. This is evident also from the transmittance versus wavelength plot, which shows almost constant transmittance of ~0.6–0.75 up to about 8.5 μm, and it decreases after 10 μm. The decrease in transmittance with an increase in the insulator (calcium fluoride) thickness, at room temperature, should be noted. This multilayered structure can be modified to be used as infrared windows in the wavelength range of 1–8.5 μm.

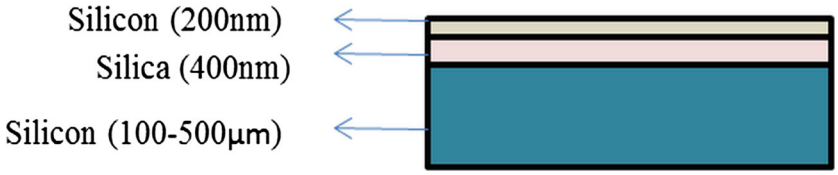

Fig. 12. SIMOX structure.

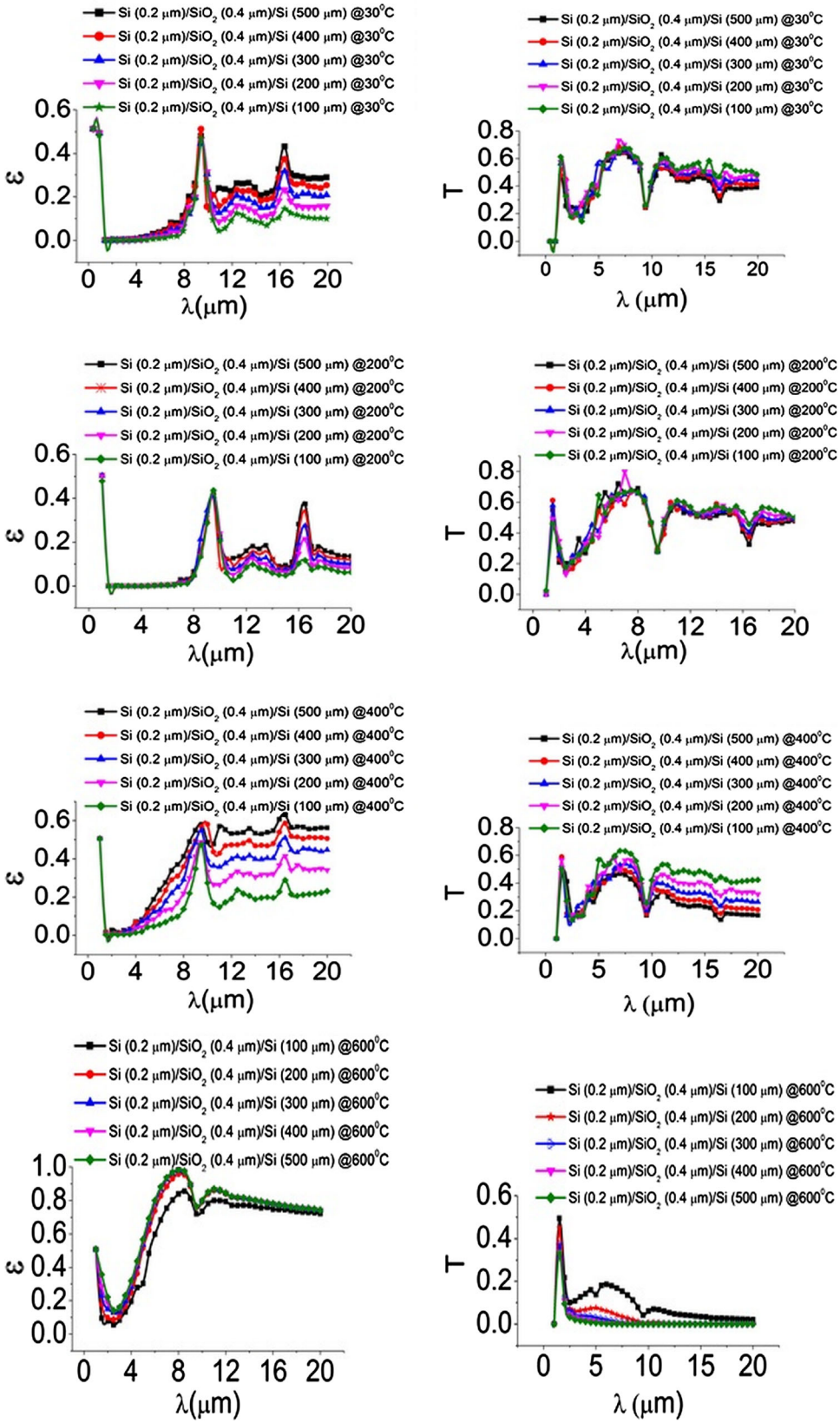

Fig. 13. Evolution of emissivity and transmittance as a function of wavelength for SIMOX at 30°C, 200°C, 400°C, 600°C, and 800°C. (Fig. 13 continued on next page.)

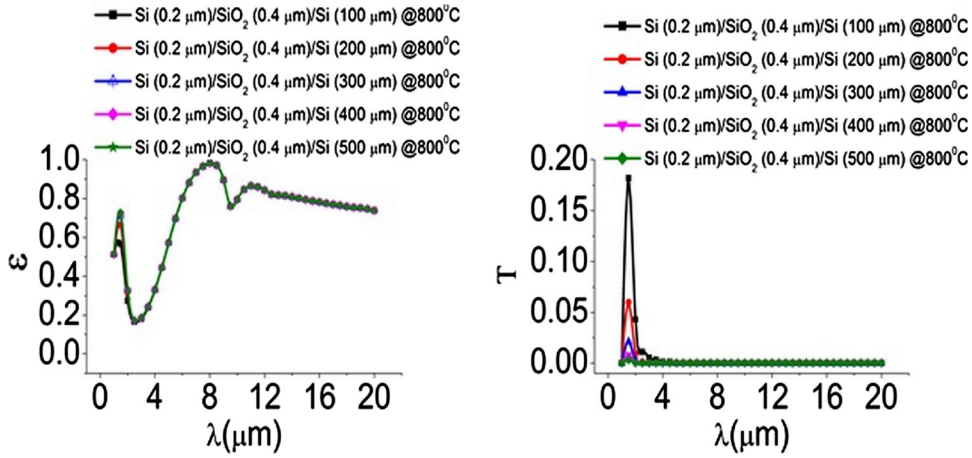

Fig. 13. Evolution of emissivity and transmittance as a function of wavelength for SIMOX at 30°C, 200°C, 400°C, 600°C, and 800°C. (Fig. 13 continued from previous page.)

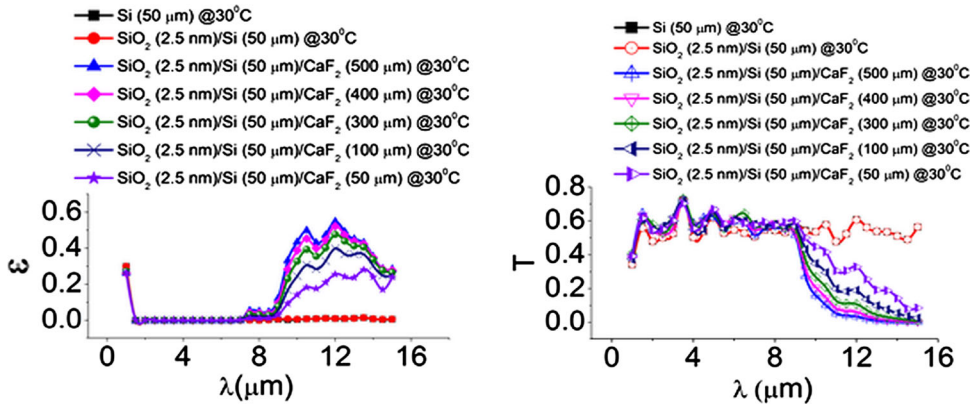

Fig. 14. Emissivity and transmittance as a function of wavelength (1–15 μm) for silicon on insulator (calcium fluoride) structure—SiO_2 (2.5 nm)/Si (50 μm)/CaF_2 (100–500 μm) (temperature in °C).

Silicon on Sapphire

We have simulated the radiative properties of SOS multilayered structure, i.e., SiO_2/Si/sapphire, as in Fig. 7, using substrate material as sapphire, varying its thicknesses from 100 μm to 500 μm, and comparing their emissivities as well as transmittance spectra in the wavelength range of 1–10 μm as shown in Fig. 15.

It is noted from Fig. 15 that SOS transmits in the wavelength range of 1.8–6.5 μm. Peak transmittance is observed in the wavelength range of ~2–6 μm with ~60% transmittance. It decreases in the wavelength range of 6–8 μm. The corresponding emissivity-versus-wavelength plot shows a strong decrease in emissivity in the wavelength range of ~2–6 μm. These structures can also be used as infrared windows.

SiO_2/Si/Graphene

This multilayered structure is simulated as in Fig. 7, with substrate material taken as graphene (1–4 layers) at room temperature and compared with silicon (50 μm) and SiO_2(2.5 nm)/Si(50 μm). The simulated emissivity as a function of wavelength for this structure is shown in Fig. 16a. It is observed that the effect of graphene is to increase the values of emissivity at a given wavelength, and its value stays linear over the entire wavelength range. The transmittance is found to decrease slightly with an increasing number of layers of graphene as shown in Fig. 16c. As shown in Fig. 16b, a sharp decrease in average reflectance from 0.45 to 0.32, at a wavelength of 1.6 μm, is observed.

A comparison of emissivity of substrate as graphite (Fig. 16d) versus graphene (Fig. 16a) indicates that the values of emissivity are much higher in the case of graphite substrate than in the case of graphene at room temperature. The emissivity changes slightly for 0.01-μm-thick graphite. In Fig. 16d, there are specific features like flat plateaus corresponding to emissivity of 0.65 for the case of graphite substrate (0.4 μm thickness). Also, a valley at a wavelength of about 1.5 μm and a peak at a wavelength of about 1.6 μm are observed for the graphite substrate.

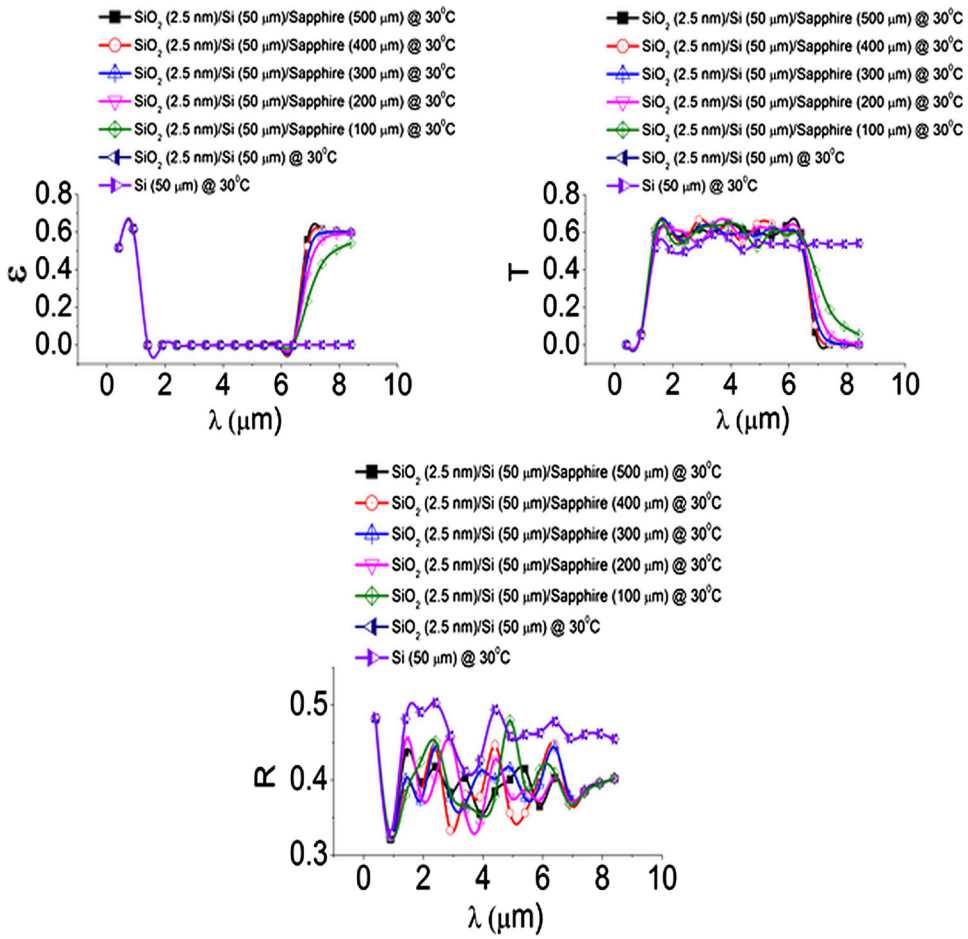

Fig. 15. Emissivity, transmittance, and reflectance for SiO_2 (2.5 nm)/Si (50 μm)/sapphire (100–500 μm) (temperature in °C).

SiO_2/Si/Graphite

We have simulated this multilayered structure as in Fig. 7. Graphite is the substrate layer with varying thicknesses of 0.01 μm, 0.1 μm, and 100 μm. Based on our simulations, above ~0.3 μm thickness of graphite, the values of emissivity are constant and independent of thickness. The values of emissivity are found to increase with an increase in thickness of graphite from 0.01 μm to 0.1 μm. The emissivity of graphite decreases above a wavelength of ~5 μm up to 20 μm, for thicknesses above 0.3 μm. These trends are shown in Fig. 17.

Graphene/SiO_2/Si

We have simulated this structure with a top layer of graphene (1–10 layers thick)/SiO_2(300 nm)/Si(50 μm). The results of emissivity and transmittance as a function of wavelength are shown in Fig. 18.

It is evident from Fig. 18 that the emissivity increases with increasing layers of graphene from 1 to 10 layers almost linearly from ~0.02 to 0.2, respectively. It is observed that the emissivity is almost constant for a particular structure within the wavelength range of 1.2–2 μm. The corresponding transmittance-versus-wavelength plots show a constant decrease in transmittance for a given wavelength as the number of layers of graphene is increased, with a peak at a wavelength of about 1.6 μm and almost constant transmittance from 1.7 μm to 2 μm.

Case 3: Device Applications

We have simulated a multilayered bolometer device configuration as shown in Fig. 19. A bolometer is a device that responds by changing its resistance due to an increase in temperature on the interaction with the incident thermal radiation.[46] When power is coupled to an electron system, electrons are driven out of thermal equilibrium along with phonons, creating hot electrons; such a bolometer is called a hot electron bolometer (HEB).[47] It is essentially a sensitive thermometer. It can be used with a spectroscope to measure the ability of some chemical compounds to absorb wavelengths of infrared radiation, by which one can obtain important information about the structure of the compounds. Because of its ability to absorb light from midinfrared to ultraviolet with nearly equal strengths, graphene

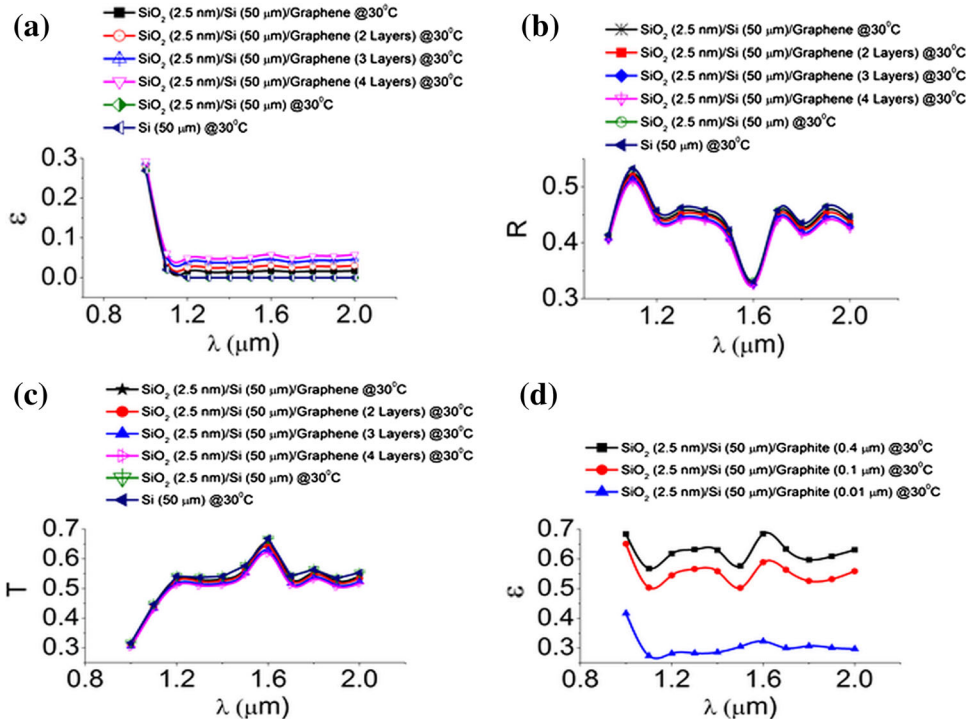

Fig. 16. (a) Emissivity, (b) reflectance, and (c) transmittance as a function of wavelength in the wavelength range of 1–2 μm for SiO_2/Si/graphene structure, and (d) emissivity as a function of wavelength in the wavelength range of 1–2 μm for SiO_2 (2.5 nm)/Si (50 μm)/graphite (0.4 μm, 0.1 μm, and 0.01 μm) (temperature in °C).

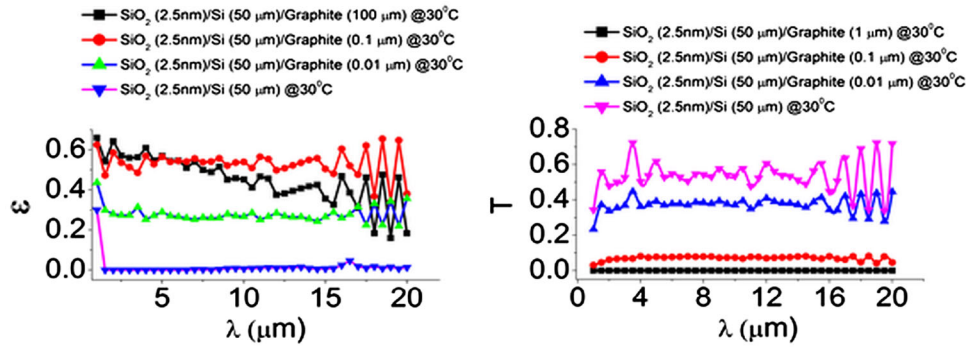

Fig. 17. Emissivity of SiO_2 (25 Å)/silicon (50 μm)/graphite (1 μm) (temperature in °C).

has found applications in optical detectors. Graphene is typically well suited for HEBs because of its small electron heat capacity and weak coupling of electrons and phonons, which causes large light-induced changes in electron temperature. Small electronic specific heat makes it possible for faster response times, higher sensitivity, and low noise equivalent power. At low temperatures, usually in the cryogenic range, electron–phonon coupling in metals is very weak. The usual range of operation of HEBs is cryogenic, whereas graphene-based HEBs can be used at higher temperatures because of the low electron–phonon scattering even at room temperature and its highest known mobilities of charge carriers at room temperature.[46,48,49]

However, the resistance of pristine graphene is weakly sensitive to electron temperature. Various approaches have been attempted to address this issue in the literature. The first one is a dual-gated bilayer graphene (DGBLG) bolometer,[50] which would have temperature-dependent resistance as well as weak electron–phonon coupling in graphene. Light absorption by DGBLG causes electrons to heat up as a result of their small electron specific heat, whereas the weak coupling of electrons and phonons helps to create a bottleneck in the heat path, decoupling the electrons from the phonon path. Good light sensitivity causes a change of resistance in the sample, which can then be converted to detectable electrical signal. The second

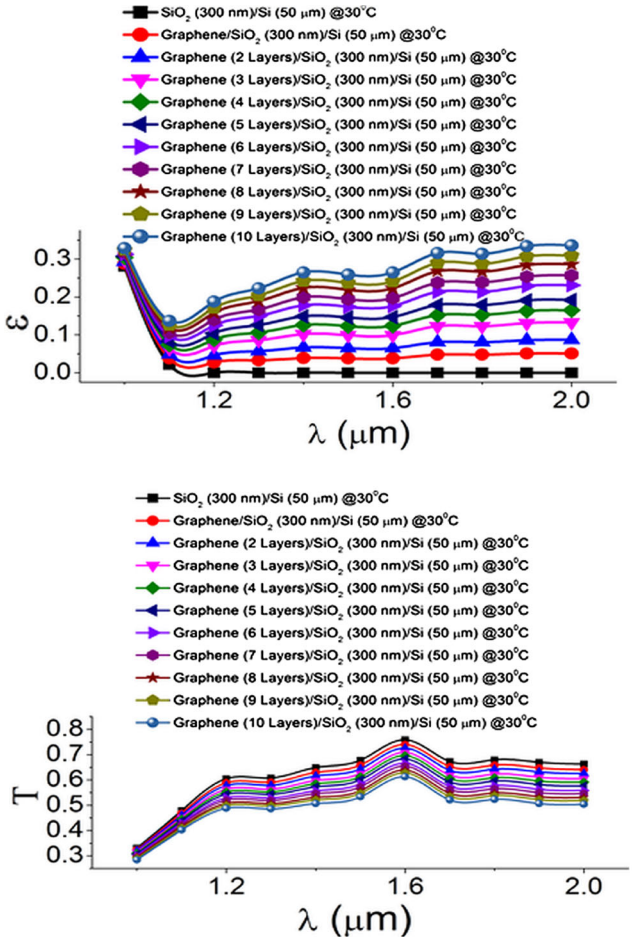

Fig. 18. Emissivity and transmittance plots for Graphene (1–10 layers)/SiO_2 (300 nm)/silicon (50 μm) (temperature in °C).

approach, which is proposed in the literature, is to use disordered graphene instead of pristine graphene. Disordered graphene has been shown to exhibit a highly temperature-dependent resistance. Also, graphene film is separated from the electrical contacts by a layer of boron nitride, which acts as a tunneling barrier to increase the contact resistance and hence thermal resistance, resulting in better thermal isolation.[46,50]

It is to be noted that to obtain higher responsivity of a device, one needs essentially to increase the absorbance of the device. Various methods for improving this characteristic are (I) multilayered graphene, (II) surface plasmonics enhancement, or (III) microcavity, with the latter two introducing selectivity of the wavelengths.[46] We have simulated two types of graphene-based hot-electron bolometer devices based on these concepts (Fig. 20).

In case 1, we simulated the bolometer structure by changing the number of layers of graphene and studying their corresponding emissivity (or absorption) to develop an understanding about its responsivity. As shown in the emissivity plot in Fig. 21, it is observed that for silicon (50 μm) and SiO_2 (0.3 μm)/Si(50 μm), the curves follow similar trends, with the latter having emissivity (or absorptance) (higher by 0.1) than the former. The emissivity (or absorptance) is found to increase for each added layer in the case of the bolometer configuration. The increase in emissivity (or absorptance) is found to be highest with copper layer of 2 nm on the top, in the wavelength range of 0.8–2 μm for the bolometer structure. This shows an improvement in the responsivity of the device. It is

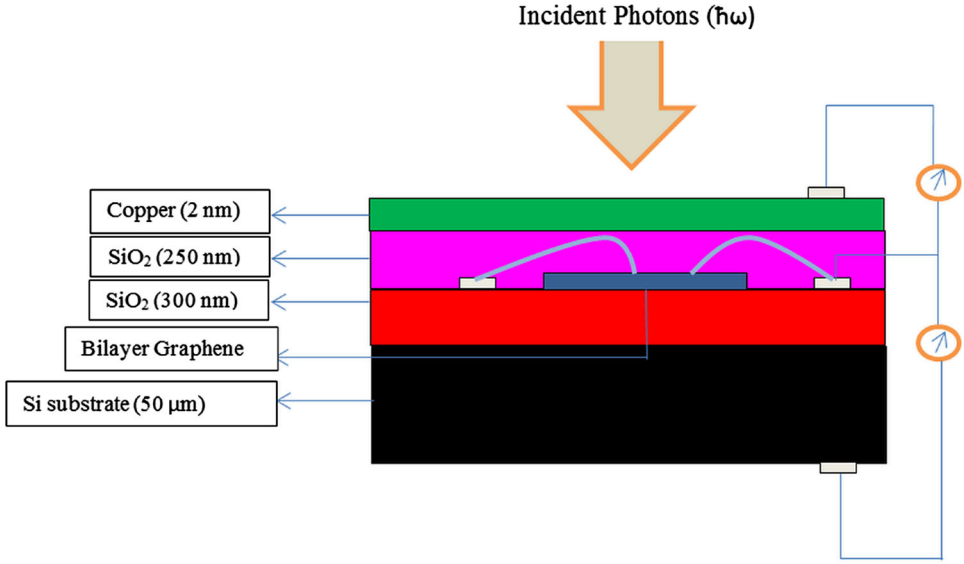

Fig. 19. Bolometer device configuration.[50]

clear that the influence of the copper layer on the top is to increase absorptance to about 20%, as compared with about 10% for the multilayered structure with corresponding reduced transmittance for the structure. Also, copper has a high temperature coefficient of resistance value (about 4.29×10^{-3}/°C)[51] and, hence, can be considered as a material that enhances the responsivity of the device by detecting a smallest change in temperature. Also, because of the layer of bilayer graphene (BLG), the device is expected to have a higher speed of response, as BLG has a lesser electron–phonon interaction and a very high mobility of electrons even at room temperature.

In case 2, graphene was shown to be an excellent material for electronic applications based on its electron transport properties. However, there are some limitations of graphene-based devices such as an induction of surface optical phonons on graphene that are in contact with substrate materials (commonly SiO_2/Si), a greater reduction in carrier mobilities than its free lying form, and the surface roughness and inhomogeneity of charge carriers.[52]

Hence, a novel approach for suppressing surface dangling bonds and surface charge traps has been proposed by using hexagonal boron nitride (h-BN) as a substrate for graphene, as h-BN has strong ionic bonding in hexagonal lattice structure. It is known that there is an ~1.7% lattice mismatch between h-BN and graphene, and hence, there is little electronic coupling with graphene. This approach has been shown to endow the device with higher electron mobilities as well as electron–hole charge inhomogeneity.

In this case, we have simulated the bolometer structure as shown in Fig. 22 based on the research by Han et al.[46] and the multilayered structure considered by Wang et al.[52] However, we have considered using pristine graphene (instead of disordered graphene) and varying the layer thicknesses of graphene and hexagonal boron nitride (h-BN) on the SiO_2/Si substrate, and we presented the evolution of their emissivity and transmittance as a function of wavelength (1–2 μm). Figure 23 shows the resistance-versus-temperature plot for this bolometer.[46] It is clear from this figure that a pristine graphene layer has a very low change in resistance with temperature. Therefore, increasing the thickness of the graphene layer can be considered as an alternative approach to increase the absorption of the device and improve its responsivity. Also, varying the thickness of BN could lead to a change in emissivity of the device and the responsivity.

As can be seen in Fig. 24a, the emissivity is found to have an increasing trend with increasing thickness of the BN layer from 20 nm to 2000 nm. The corresponding optical transmittance is found to decrease with an increasing thickness of the BN layer as shown in Fig. 24b.

Furthermore, we consider the thickness of boron nitride layer as 2 nm on the SiO_2/Si substrate. We note that with an increasing number of layers of graphene, up to 10 layers, the emissivity of the device structure increases and a corresponding decrease is observed in the optical transmittance with respect to bare substrate (Fig. 25). This is indicative of the improved device performance as a bolometer. This is because, on increasing the number of layers of graphene, we expect the resistance of

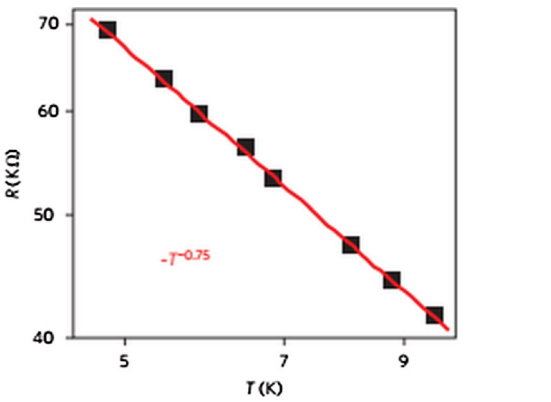

Fig. 20. Resistance as a function of temperature for BLG bolometer.[50]

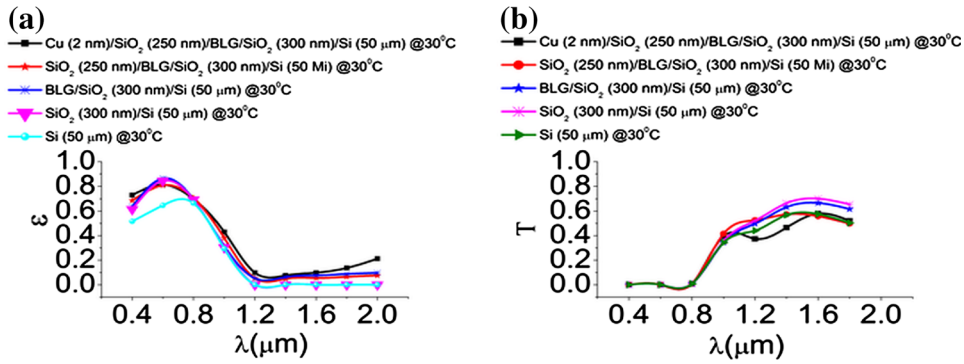

Fig. 21. Emissivity (or absorptance) and transmittance as a function of wavelength for the various layers in the proposed bolometer configuration (temperature in °C).

the structure to change more effectively with temperature (like in the case of graphite).

Another approach to address the issue of increasing the ratio of change in resistance with temperature is to replace the top layer of graphene with graphite, which has a higher ratio of change in resistance with temperature. It can act as a good absorber of the incoming radiation, leading to better performance of the bolometer. Figure 26 shows the trends in emissivity as increasing with the thickness of graphite in the wavelength range of 1–2 μm. Graphite with a thickness of 0.01 μm is found to have the highest emissivity in the wavelength range of 1.5–2 μm. The emissivity is the highest for graphite with a thickness of 1 μm in the wavelength range of 1–1.5 μm. Emissivity trends are generally found to be linear with little variations with wavelength for a given substrate for near IR.

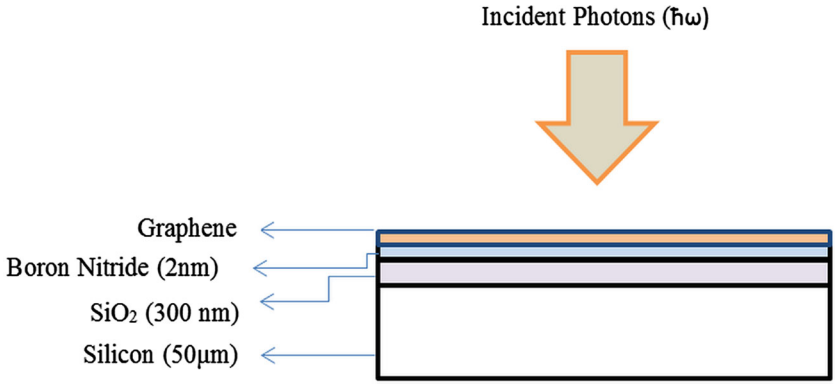

Fig. 22. Bolometer device structure with multilayered configuration graphene/BN/SiO_2/Si.

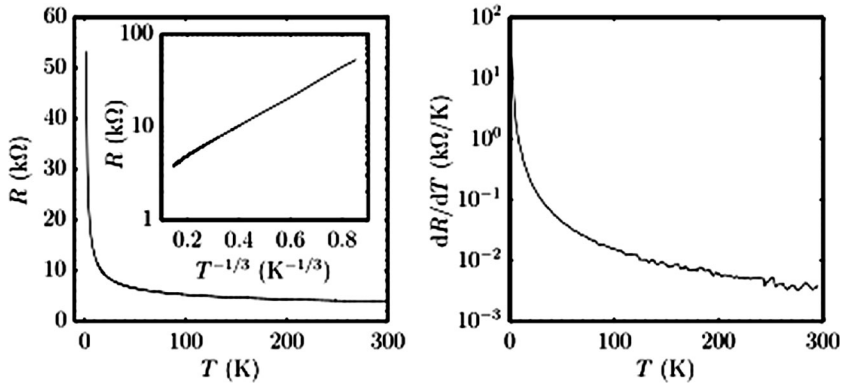

Fig. 23. Temperature dependence of resistance of graphene-nanoribbon-based bolometer device.[46]

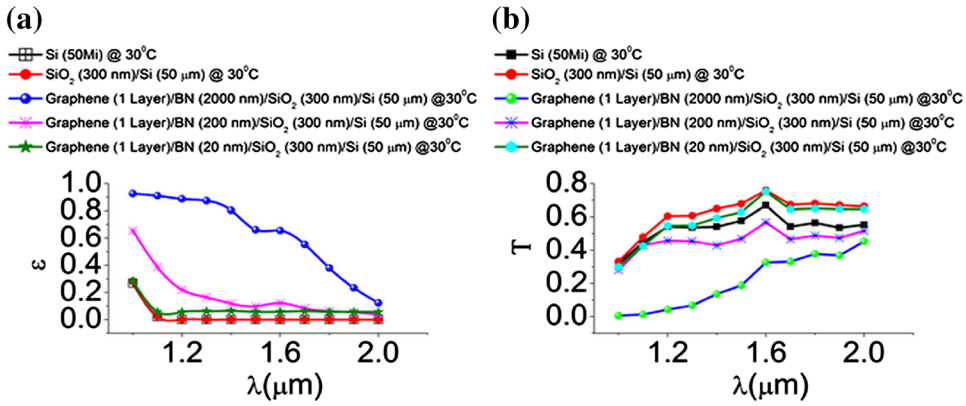

Fig. 24. Effect of variation of BN thickness on the (a) emissivity and (b) transmittance of bolometer structure configuration (temperature in °C).

Figure 27 shows the effect of a variation of graphite thickness on emissivity and transmittance in the wavelength range of 1–20 μm. For a lower thickness of graphite (0.001 μm), emissivity and transmittance follow similar trends as the substrate SiO_2/Si with little increase in the value of emissivity in the wavelength range of 1–20 μm. With increasing the thickness of graphite above 0.5 μm, the trends of emissivity and transmittance are found to be constant and are independent of thickness. Increasing trends in emissivity indicate better responsivity of the device.

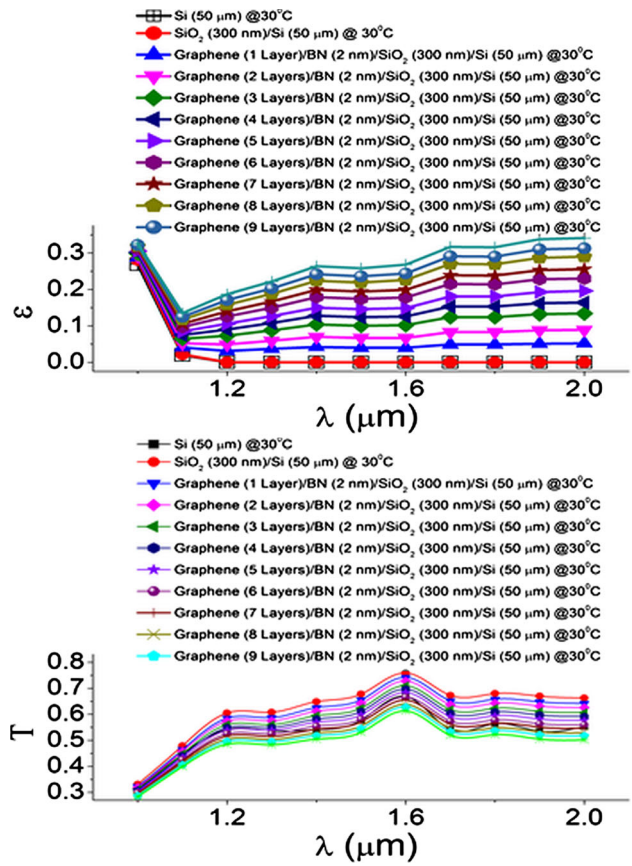

Fig. 25. Effect of change of thickness of graphene on emissivity and transmittance as a function of wavelength (1–2 μm) (temperature in °C).

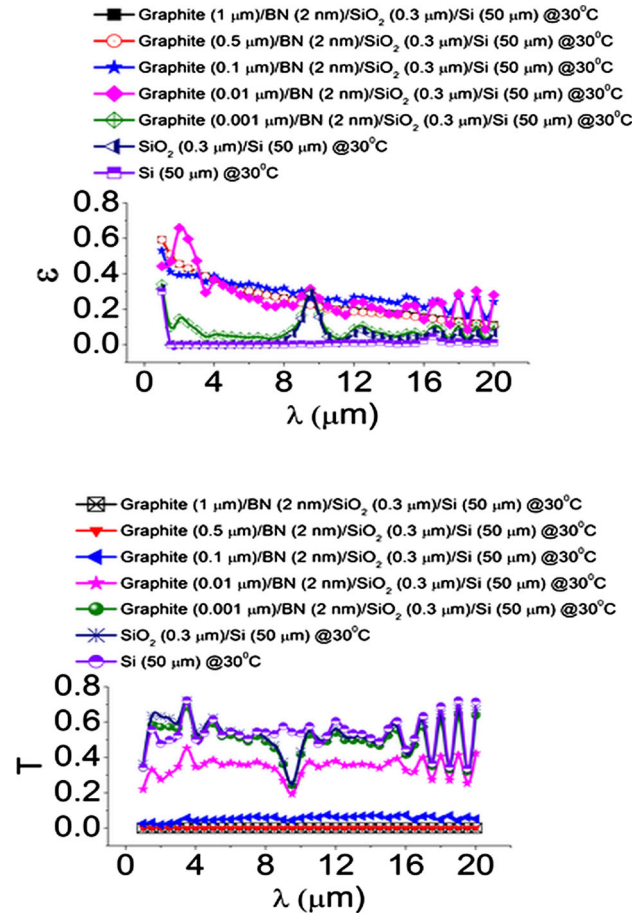

Fig. 27. Effect of change of thickness of graphite on emissivity and optical transmittance as a function of wavelength (1–20 μm) for bolometer configuration (temperature in °C).

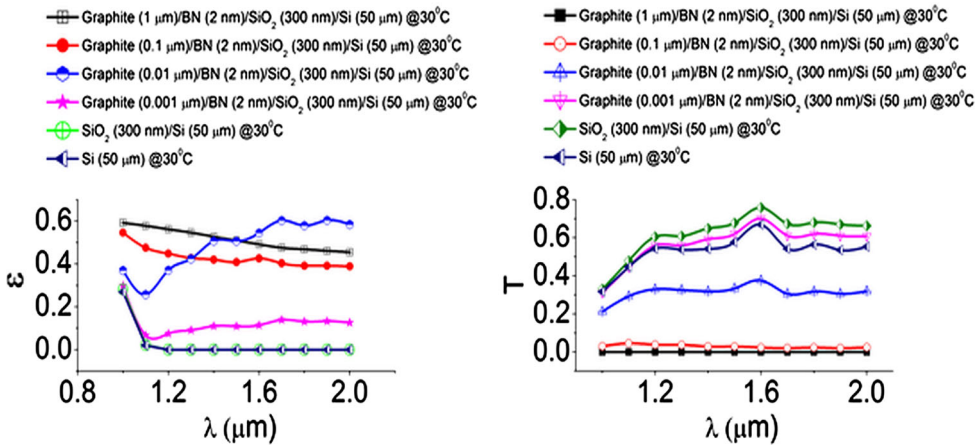

Fig. 26. Effect of change of thickness of graphite on the emissivity and optical transmittance as a function of wavelength (1–2 μm) (temperature in °C).

CONCLUSIONS

A comparison of the wavelength- and thickness-dependent optical properties, mainly emissivity and transmittance, has been presented for various bulk electronic materials, coatings, and a graphene-based bolometer. Because of its metallic characteristics, aluminum is found to have lower emissivity than silicon in the wavelength range of 1–20 μm. With increasing thickness, the emissivity of silicon increases. Diamond exhibits thickness-dependent emissivity and saturates at 0.6 for thickness of 5000 μm and above. Graphite is found to have emissivity that is independent of thicknesses. The emissivity of graphene remains low and increases with an increase in the number of layers. Sapphire and CaF_2 exhibit high transmittance and, as is known, are ideal candidates for infrared windows. In the wavelength range of 1–20 μm, SiC is found to have emissivity that is independent of thickness above 500 μm. The emissivity of GaN is independent of thickness above 5 μm.

Multilayered structures such as SOD, SOS, SIMOX, silicon on insulator, silicon on graphene, silicon on graphite, and graphene on silicon have been shown to have different emissivities as a function of wavelength, thickness, and temperature. An investigation into the infrared properties of graphene-based bolometer has been presented. In the case of a dual-gated graphene bolometer, it is found that the emissivity increases with the addition of layers. Copper is found to improve the responsivity of the device. For a BN-based hot-electron bolometer, the emissivity is found to increase with an increase in BN layer thickness. The effect of graphene is to increase the emissivity of the bolometer structure. A comparison of the emissivity of graphite and graphene shows that graphite exhibits higher emissivity.

ACKNOWLEDGEMENTS

Work on emissivity measurements and modeling, at NJIT, began in the 1990s. The work was sponsored by the Defense Advanced Research Projects Agency (DARPA, under the Microelectronics Manufacturing Science and Technology [MMST] Program with Dr. Arati Prabhakar, now Director, DARPA and the late Mr. Raymond S. Balcerak, Program Manager at DARPA), Department of Defense–University Research Instrumentation Program (DOD-DURIP), and SEMATECH. This work is dedicated to Mr. Balcerak, his leadership, and his vision.

REFERENCES

1. Z.M. Zhang, B.K. Tsai, and G. Machin, *Radiometric Temperature Measurements: Experimental Methods in Physical Sciences*, ed. Z.M. Zhang, B.K. Tsai, G. Machin, A.C. Parr, and T. Lucatorto (Salt Lake City, UT: Academic Press, 2010), pp. 217–271.
2. L. Michalski, K. Eckersdorf, J. Kucharski, and J. McGhee, *Temperature Measurement*, ed. L. Michalski, K. Eckersdorf, J. Kucharski, and J. McGhee (Oxford, UK: Wiley, 2001), pp. 1–18.
3. *Platinum Resistance Temperature Detectors,* Honeywell, 2014, https://www.honeywellprocess.com/en-US/explore/products/instrumentation/temperature-sensors/Pages/platinum-resistance-temperature-detectors.aspx.
4. H. Chang, *Inventing Temperature: Measurement and Scientific Progress*, ed. P. Humphreys (London, UK: Oxford University Press, 2004), pp. 159–217.
5. R.E. Bentley, *Temperature and Humidity Measurement*, ed. R.E. Bentley (New York: Springer-Verlag Singapore Pte. Ltd, 1998), pp. 81–103.
6. T.A. Hughes, *Measurement and Control Basics*, ed. T.A. Hughes (Research Triangle Park, NC: ISA—The Instrumentation, Systems, and Automation Society Press, 2002), pp. 171–197.
7. P.J. Timans, R.A. McMahon, and H. Ahmed, *Appl. Phys. Lett.* 53, 1844 (1988).
8. S. Wolf and R.N. Tauber, *Silicon Processing for the VLSI Era, Volume 1—Process Technology*, ed. S. Wolf and R.N. Tauber (Sunset Beach, CA: Lattice Press, 1986), pp. 36–72.
9. T. Borca-Tascuic, D.A. Achimov, and G. Chen, *Mater. Res. Soc. Symp. Proc.* 525, 103 (1998).
10. J. Wagner and F.G. Boebel, *Mater. Res. Soc. Symp. Proc.* 429, 303 (1996).
11. N.M. Ravindra, B. Sopori, O.H. Gokce, S.X. Cheng, A. Shenoy, L. Jin, S. Abedrabbo, W. Chen, and Y. Zhang, *Int. J. Thermophys.* 22, 1593 (2001).
12. W.F. Kosonocky, M.B. Kaplinsky, N.J. McCaffrey, E.S.H. Hou, C.N. Manikopoulos, N.M. Ravindra, S. Belikov, J. Li, and V. Patel, Infrared detectors and focal plane arrays III. *Proc. SPIE* 2225, 26 (1994).
13. M.B. Kaplinsky, J. Li, N.J. McCaffrey, V. Patel, E.S.H. Hou, N.M. Ravindra, C.N. Manikopoulos, and W.F. Kosonocky, *Opt. Eng.* 36, 3176 (1997).
14. M. Willander, M. Friesel, Q. Wahab, and B. Straumal, *J. Mater. Sci. Mater. Elect.* 17, 1 (2006).
15. N.M. Ravindra, S. Abedrabbo, O.H. Gokce, F. Tong, A. Patel, R. Velagapudi, G.D. Williamson, and W.P. Maszara, *IEEE Trans. Compon. Packag. A* 21, 441 (1998).
16. E. Dziubakiewicz and B. Buszewski, *Electromigration Techniques: Theory and Practice*, ed. B. Buszewski, D. Ewelina, and S. Michal (Berlin, Germany: Springer-Verlag, 2013), pp. 5–26.
17. M. Repeta, J. Kolk, M. Saran, and V.Q. Ho, *VLSI Multilevel Interconnection Conference Proceedings*, 351 (1990).
18. J.P. Colinge, *Silicon-on-Insulator Technology: Materials to VLSI*, ed. J.P. Colinge (New York: Springer Science + Business Media, LLC, 2004), pp. 9–68.
19. S.H. Voldman (ed.), *Latchup* (New York: Wiley, 2007), pp. 1–46.
20. A. Aleksov, J.M. Gobien, X. Li, J.T. Prater, and Z. Sitar, *Diam. Relat. Mater.* 15, 248 (2006).
21. A. Soderbarg, B. Edholm, J. Olsson, S. Tiensuu, and E. Johansson, *SOI Conference Proceedings* (Piscataway, NJ: IEEE International, 1993), pp. 58–59.
22. A. Soderbarg, B. Edholm, and S. Bengtsson, *SOI Conference Proceedings* (Piscataway, NJ: IEEE International, 1995), pp. 104–105.
23. C. Gu, Z. Jin, X. Lu, G. Zou, C. Wang, J. Lu, D. Yao, X. Su, and Z. Xu, *Diam. Relat. Mater.* 7, 753 (1998).
24. D. Flandre, A.N. Nazarov, and P.L.F. Hemment, *Proceedings of the NATO Advanced Research Workshop on Science and Technology of Semiconductor-On-Insulator Structures and Devices Operating in a Harsh Environment*, ed. D. Flandre, A.N. Nazarov, and P.L.F. Hemment (Kiev, Ukraine: Kluwer Academic, 2005).
25. T.-J. Hsiao, T. Eyassu, K. Henderson, T. Kim, and C.-T. Lin, *Nanotechnology* 24, 395401 (2013).
26. K. Novoselov, A. Geim, S. Morozov, D. Jiang, Y. Zhang, S. Dubonos, I. Grigorieva, and A. Firsov, *Science* 306, 666 (2004).
27. L. Yu-Ming, C. Hsin-Ying, K.A. Jenkins, D.B. Farmer, P. Avouris, and A. Valdes-Garcia, *Electron Devices Lett., IEEE* 31, 68 (2010).
28. A.N. Grigorenko, M. Polini, and K.S. Novoselov, *Nat. Photonics* 6, 749 (2012).
29. A.K. Geim and K.S. Novoselov, *Nat. Mater.* 6, 183 (2007).

30. G.A. Slack, *Phys. Rev.* 122, 1451 (1961).
31. J.W. Ekin, *Experimental Techniques for Low-Temperature Measurements: Cryostat Design, Material Properties and Superconductor Critical-Current Testing*, ed. J.W. Ekin (Oxford, UK: Oxford University Press, 2006), pp. 248–252.
32. *Sapphire* (Al_2O_3), CRYSTRAN, 2014, http://www.crystran.co.uk/optical-materials/sapphire-al2o3.
33. D. Cattelan, C. Eypert, M. Kloul, M. Gaillet, J.-P. Gaston, R. Seitz, A. Shagaleeva, and M. Stchakovsky, *Ellipsometry at the Nanoscale*, ed. M. Losurdo and K. Hingerl (Berlin, Germany: Springer-Verlag, 2013), pp. 629–667.
34. N.A. O'Brien, J. Gordon, H. Mathew, and B.P. Hichwa, *Thin Solid Films* 345, 312 (1999).
35. M. Irie, Y. Yokoyama, and T. Seki, *New Frontiers in Photochromism*, ed. M. Irie, Y. Yokoyama, and T. Seki (Tokyo, Japan: Springer, 2013), p. 13.
36. A. Yariv and P. Yeh, *Optical Waves in Crystals* (New York: Wiley, 1984), pp. 155–219.
37. R. Siegel and J.R. Howell, *Thermal Radiation Heat Transfer* (New York: Hemisphere Publishing Corporation, 2001), pp. 683–734.
38. N.M. Ravindra, K. Ravindra, S. Mahendra, B. Sopori, and A.T. Fiory, *J. Electron. Mater.* 32, 1052 (2003).
39. J.P. Hebb and K.F. Jensen, *J. Elect. Soc.* 143, 1142 (1996).
40. A. Petersson (Uppasala Universitet, 2011), p. 50.
41. E.D. Palik (ed.), *Handbook of Optical Constants of Solids*, (Waltham, MA: Academic Press, 1998), pp. 275–798.
42. A.M. Zaitsev, *Optical Properties of Diamond: A Data Handbook*, ed. A.M. Zaitsev (Berlin, Germany: Springer, 2001), pp. 1–9.
43. J.W. Weber, V.E. Calado, and M.C.M. van de Sanden, *Appl. Phys. Lett.* 97, 091904 (2010).
44. P. Avouris, *Nano Lett.* 10, 4285 (2010).
45. W.G. Spitzer, D.A. Kleinman, C.J. Frosch, and D.J. Walsh, *Silicon Carbide: A High Temperature Semiconductor*, ed. J.R. O'Connor and J. Smiltens (Boston, MA: Pergamon Press, 1959), pp. 347–365.
46. Q. Han, T. Gao, R. Zhang, Y. Chen, J. Chen, G. Liu, Y. Zhang, Z. Liu, X. Wu, and D. Yu, *Sci. Rep.* 3, 6 (2013).
47. D. Gu, *Electrical Engineering* (Ann Arbor, MA: University of Massachusetts Amherst, 2007), p. 174.
48. S.V. Morozov, K.S. Novoselov, M.I. Katsnelson, F. Schedin, D.C. Elias, J.A. Jaszczak, and A.K. Geim, *Phys. Rev. Lett.* 100, 016602 (2008).
49. S.S. Kubakaddi, *Phys. Rev. B* 79, 075417 (2009).
50. Y. Jun, H. Kimm, J.A. Elle, B. Sushkova, G.S. Jenkins, H. Milchberg, M.S. Fuhrer, and H.D. Drew, *Nat. Nanotechnol.* 7, 472 (2012).
51. *Resistivity, Conductivity and Temperature Coefficients for some Common Materials,* The Engineering ToolBox, 2014, http://www.engineeringtoolbox.com/.
52. M. Wang, S.K. Jang, W.-J. Jang, M. Kim, S.-Y. Park, S.-W. Kim, S.-J. Kahng, J.-Y. Choi, R.S. Ruoff, Y.J. Song, and S. Lee, *Adv. Mater.* 25, 2746 (2013).